◎ 논 문
◎ Original Paper

DOI: https://doi.org/10.5293/kfma.2026.29.1.061
ISSN (Print): 2287-9706

세미오픈 케이싱 적용 사류펌프의 기동 운전 성능을 고려한 임펠러 형상 최적화

쉬레스트 우즈왈* · 김정열** · 최영도***†

Impeller shape optimization considering start-up operation performance of mixed flow pump with semi-open casing

Ujjwal Shrestha*, Jeongyeol Kim**, Young-Do Choi***†

Key Words : Mixed Flow Pump (사류펌프), Semi-open Casing (세미오픈 케이싱), Pump Performance (펌프 성능), Start-up Operation (기동 운전 성능), Optimization (최적화)

ABSTRACT

Mixed flow pumps play a crucial role in fluid transportation by integrating centrifugal and axial flow principles to achieve high flow rates and moderate head conditions. However, their efficiency and hydraulic stability can be compromised by challenges such as impeller blade misalignment, vortex formation, hump characteristics, and transient instabilities during start-up. One of the most effective ways to optimize pump performance is through the use of advanced computational techniques that refine impeller design, particularly blade angles, to enhance efficiency and suppress undesirable flow phenomena. Computational Fluid Dynamics (CFD), Response Surface Modeling (RSM), and Multi-Objective Genetic Algorithm (MOGA) are integrated to obtain the optimal impeller design. The optimal impeller design showed better performance and hump characteristics from start-up to design rotational speed.

1. Introduction

Mixed flow pumps are crucial in industrial fluid transportation, offering high flow rates with moderate head conditions. They integrate centrifugal and axial flow principles to move large fluid volumes effectively while maintaining pressure stability[1]. Commonly used in agricultural irrigation, municipal water supply systems, flood control, and thermal power plant cooling, these pumps provide reliability in demanding environments[2]. However, challenges such as impeller blade misalignment, vortex formation, hump characteristics, transient instabilities during start-up, and variable speed performance can impact efficiency, hydraulic stability, and durability, contributing to increased maintenance needs[3]. Impeller blade misalignment disrupts the uniformity of fluid movement, leading to uneven pressure distribution, turbulence, and localized energy losses[4].

To address these challenges, researchers have explored optimized blade curvature and diffuser designs to suppress vortex formation, thereby promoting smoother fluid movement and conserving energy[5]. One of the unique phenomena affecting mixed-flow pumps is the hump characteristic, which manifests as an abnormal fluctuation in the flow-head curve. Often

* Institute of New and Renewable Energy Technology Research, Mokpo National University
** MA-Tech, Co., Ltd.
*** Department of Mechanical Engineering, Institute of New and Renewable Energy Technology Research, Mokpo National University
† 교신저자, E-mail : ydchoi@mnu.ac.kr

linked to rotating stall conditions, this behavior leads to energy dissipation, increased vibration, and noise, resulting in operational instability in high-speed pumps. The hump characteristic typically emerges under partial load conditions due to internal vortex structures, where the impeller's work capacity declines while internal fluid losses increase[6]. Ji et al.[2] investigated entropy production mechanisms in the hump region, revealing that variations in pressure and velocity distributions contribute to performance degradation. Similarly, Li et al.[7] analyzed the rotating stall phenomenon using the SST turbulence model. Furthermore, rotating stall can be mitigated by refining impeller blade profiles, adjusting guide vanes, and implementing active flow control strategies to stabilize pump operation and reduce energy losses[8].

Pump start-up is a critical phase that significantly influences overall system stability. Transient flow conditions during this period can induce sudden pressure fluctuations, shaft vibrations, and flow-induced noise, making it essential to refine start-up protocols for optimal performance[9]. Additionally, variable rotational speed operations allow mixed flow pumps to accommodate fluctuating demand while enhancing energy efficiency. Speed conversion strategies—such as linear acceleration, quadratic power-based speed conversion, and segmented adjustments—affect shaft vibrations and hydraulic performance. Advanced control systems, such as variable frequency drives (VFDs), dynamically regulate pump speed, thereby reducing energy consumption while maintaining efficiency and stability[10]. Understanding pump behavior at low rotational speeds can help improve start-up performance.

Optimization techniques such as Computational Fluid Dynamics (CFD), Response Surface Modeling (RSM), and Genetic Algorithms (GA) help improve impeller design for performance[11]. CFD simulations enable detailed analysis of fluid interactions, allowing for refinements in impeller geometry, blade angles, and design parameters to minimize turbulence and hydraulic losses. Huang et al. use blade loading distribution as design parameters to perform optimization of a mixed flow pump impeller[12]. Chen et al. used hydrodynamic and geometric parameters for the optimization and performance improvement of the mixed flow pump[13]. Bonaiuti and Zangeneh used the 3D inverse method to parameterize the blade geometry[14]. RSM modeling establishes correlations between design parameters and objective functions. Genetic algorithms provide an iterative optimization framework, selecting optimal impeller configurations to enhance stability and performance[15].

This study aims to evaluate the performance of a mixed flow pump with a semi-open casing, with particular emphasis on start-up operational conditions. To address the start-up phase, the pump is analyzed across a range of rotational speeds, from low to high. The design of the mixed flow pump is intended to achieve optimal performance during start-up. The internal flow behavior observed during start-up closely resembles that of low-speed operation. Additionally, blade angles are selected as parameters for the impeller design. Response Surface Methodology (RSM) and Genetic Algorithm (GA) are integrated to optimize the impeller design and enhance pump performance across various operating conditions, including rotational speed and flow rate.

2. Design and Numerical Analysis

2.1 Design Methodology

The impeller with semi-open casing geometry is designed according to the previous theory. The mixed flow pump is designed based on a specific speed.

The specific speed of the mixed flow pump is 810 [min^{-1}, m, m^3/s], which is calculated at the design point. Table 1 shows the detailed specifications of the mixed flow pump.

$$N_s = \frac{N\sqrt{Q}}{H^{0.75}} \tag{1}$$

Table 1 Design specification of mixed flow pump

Parameters	Values
Head, H	45 m
Flow rate, Q	150 m^3/min
Rotational speed, N	1150 min^{-1}
Specific speed, N_S	810 m-m^3/min^{-1}
Casing inner radius, r_c	300 mm
Number of blades, z	5

where N_s is the specific speed of the pump (m−m^3/min^{-1}), N is the rotational speed (min^{-1}), H is the effective head (m), Q is the flow rate (m^3/s).

Fig. 1 illustrates a 3D model of the mixed flow pump with a semi−open casing. Fluid enters axially through the inlet pipe and exits radially from the impeller. Fig. 2 presents the meridional shape of the mixed flow pump, highlighting key geometric parameters. In this figure, d represents the impeller diameter, while b denotes the impeller width. Subscripts 1 and 2 indicate the inlet and outlet of the impeller, respectively. These design parameters play a fundamental role in determining the overall performance curves of the mixed flow pump.

Fig. 3 depicts the flow passage of the mixed flow

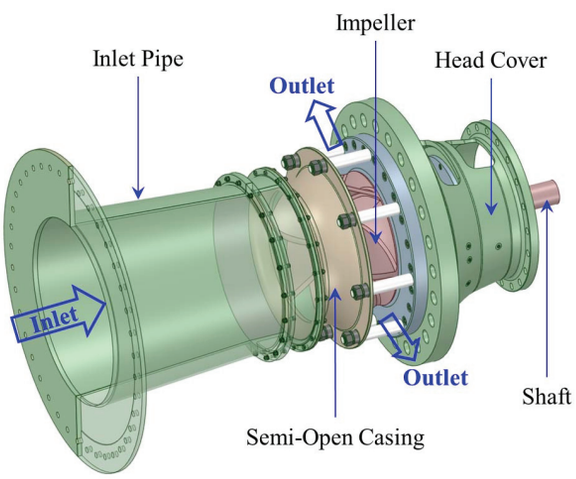

Fig. 1 3D model of a mixed flow pump with semi−open casing

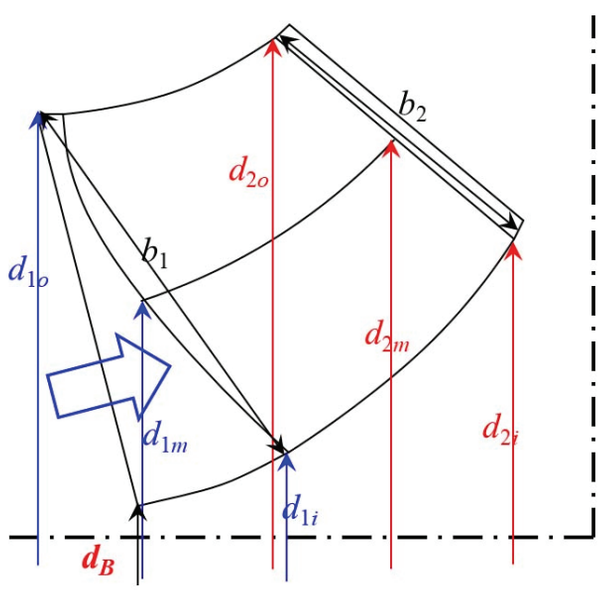

Fig. 2 Parametric design of mixed flow pump impeller

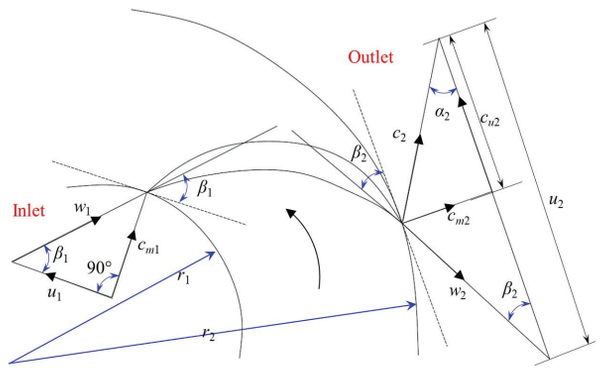

Fig. 3 Theoretical calculation of inlet and outlet blade angle

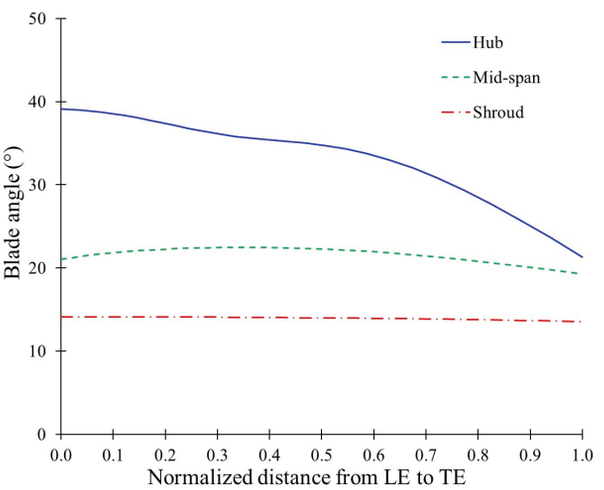

Fig. 4 Blade angle distribution of the initial impeller blade design of a mixed flow pump

pump, along with inlet and outlet velocity triangles. The inlet blade angle (β_1) and outlet blade angle (β_2) are derived from these velocity triangles and serve as crucial design variables that influence pump performance. Proper selection of these angles is essential for optimizing impeller blade design. Fig. 4 illustrates the blade angle distribution of the initial impeller from the leading edge (LE) to the trailing edge (TE).

2.2 Numerical Methodology

The commercial software ANSYS 2024R1[16] is employed to perform steady−state and unsteady−state numerical analyses of the mixed flow pump with a semi−open casing. The Reynolds−Averaged Navier−Stokes (RANS) equations are used to solve the incompressible flow within the mixed flow pump. The accuracy of the numerical simulation depends on the quality of the

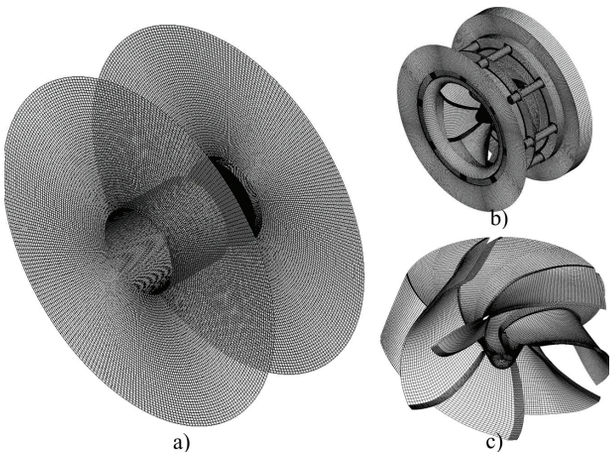

Fig. 5 Numerical grids for mixed flow pump a) full domain, b) impeller with semi-open casing, and c) initial impeller blades

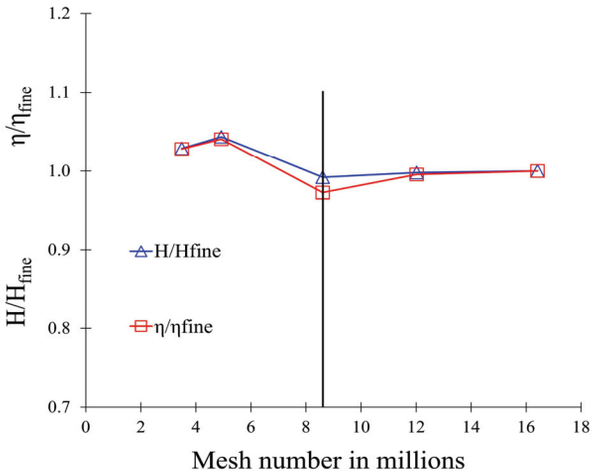

Fig. 7 Mesh dependency test for an initial impeller of mixed flow pump at $Q/Q_D = 1.00$

numerical grid. Fig. 5 presents the numerical grids used for the mixed flow pump with a semi-open casing, and ANSYS ICEM 2024R1 is employed for grid generation. Due to flow separation and reattachment within the boundary layers along the impeller wall, a refined mesh layer is necessary.

The y^+ value for the mixed flow pump remains below 50 to ensure a smooth transition within the boundary layer. The Shear Stress Transport (SST) turbulence model, equipped with automatic near-wall treatment, facilitates a seamless transition from the low-Reynolds-number formulation to the wall-function approach in hydraulic machinery analysis[17].

Fig. 6 illustrates the boundary conditions for the mixed flow pump with a semi-open casing. A mesh dependency test is conducted to determine the optimal grid size for stable CFD analysis. Fig. 7 displays the mesh dependency test for the mixed flow pump at $Q/Q_D = 1.0$, confirming that 8.6 million nodes are suitable for CFD analysis. For the mixed flow pump simulation, static pressure is set at the inlet, while mass flow rate is defined at the outlet. A frozen rotor and transient rotor-stator interface models are selected for steady and unsteady state analysis, respectively.

The performance curve is generated by varying the mass flow rate at the pump outlet. The simulation achieves convergence once the RMS residuals of the continuity and momentum equations fall below 1×10^{-6}. Additionally, FSI analysis evaluates the structural stability of the mixed flow pump impeller. The boundary conditions for FSI analysis are adapted from a previous study[18] to evaluate the structural stability of the mixed flow pump impeller.

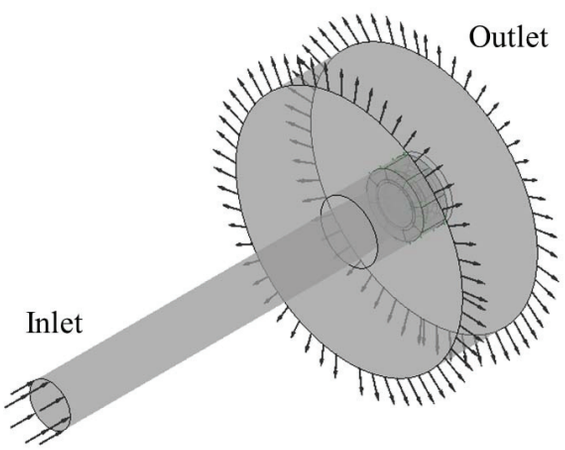

Fig. 6 Boundary conditions for the mixed flow pump with semi-open casing

2.3 Optimization Methodology

The impeller design optimization for a mixed flow pump with a semi-open casing requires a systematic approach to enhance hydraulic performance, with the blade angle being the key parameter. Fig. 8 illustrates the optimization methodology for the mixed flow pump.

In a mixed flow pump, significant energy loss occurs within the impeller. These losses are primarily due to sudden changes in flow direction and uneven velocity distribution, which lead to vortex formation. The impeller blade angle and curvature play a critical role

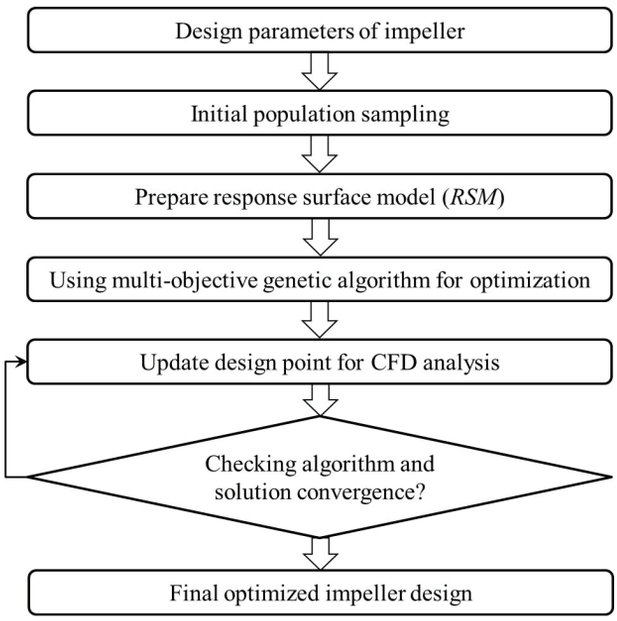

Fig. 8 Optimization methodology for mixed flow pump impeller

in controlling flow direction and efficiency. The optimization process begins with defining the blade angle, which plays a crucial role in pressure distribution, energy transfer, and overall pump efficiency. Hence, the blade angle is selected as the primary design variable for optimization. Fig. 9 shows the blade angle distribution at the hub and shroud region. The 4 control points on the hub and shroud are selected to control the blade curvature and flow direction. A total of 8 design variables are selected for the impeller design optimization of the mixed flow pump. The selection of upper and lower bounds is necessary for

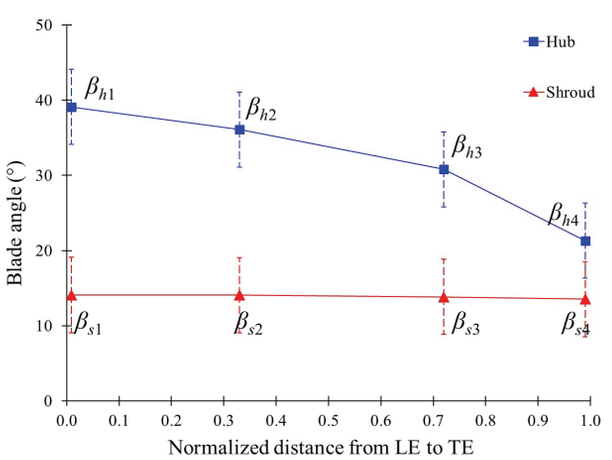

Fig. 9 Design variables of the initial impeller of the mixed flow pump

Table 2 Upper and lower bounds of design variables of mixed flow impeller

Design Variables	Lower Bound	Upper Bound
β_{h1}	30°	45°
β_{h2}	25°	50°
β_{h3}	20°	40°
β_{h4}	10°	35°
β_{s1}	8°	20°
β_{s2}	8°	20°
β_{s3}	8°	20°
β_{s4}	8°	20°

the optimization space. Table 2 shows the upper and lower bounds of the mixed flow pump for the design samples. While selecting the upper and lower bounds, the parametric study was performed. The change in blade angle of the mixed flow pump directly influenced efficiency and head curve. The objective of optimization is to enhance the hydraulic performance and improve the hump characteristic of the mixed flow pump with a semi-open casing.

A well-distributed and diverse design variation is needed for a proper Design of Experiment (DOE) set. Optimal Space Filling (OSF) is utilized for initial population sampling. OSF strategically selects design points across the parameter space to minimize clustering and improve the accuracy of subsequent simulations, reducing computational costs while maintaining reliable results. The OSF generated blade angle configurations and CFD simulations analyze performance and flow behavior. The data from these simulations are used to construct a Response Surface Model (RSM) to predict the correlation between design variables and objective functions. Genetic Aggregation RSM combines multiple response surface models to improve prediction accuracy and interactions between design parameters and objective functions.

The Multi-Objective Genetic Algorithm (MOGA) is applied using the optimization formulation shown in Table 3, with hydraulic efficiency, flow uniformity, and pressure ratio selected as the objective functions to quantify the mixed flow pump performance and internal flow. Flow uniformity was evaluated by analyzing the consistency of pressure and velocity distributions across the flow field, providing insight into the fluid behavior within the pump system[19,20].

Table 3 Optimization formulation for mixed flow pump impeller

Design Variables	$x_{imp} = [\beta_{h1},...,\beta_{h4}, \beta_{s1},..., \beta_{s4}]^T$
Objective functions	$\eta(x_{imp}) = \frac{\rho g Q H}{T\omega}$
	$\gamma(x_{imp})_{out} = 1 - \oint \frac{\sqrt{(\bar{u}-u)^2}}{2A\bar{u}} dA$
	$p_{ratio} = \frac{p}{p_{\max}}$
Constraints	$p_{out}(x_{imp}) < 10bar$
	$\eta(x_{imp}) > 72\%$
	$Q/Q_D(x_{imp}) = 0.5$
	$\beta_{h1} \geq \beta_{m1} \geq \beta_{s1}$

where, $\eta(x_{imp})$ is hydraulic efficiency, $\gamma(x_{imp})$ is flow uniformity and p_{ratio} is pressure ratio for a mixed flow pump with semi-open casing. $\bar{u}$ and u are average and local velocity at the cross-sectional area, A, respectively. p and $p_{\max}$ are the local and the maximum pressure at the outlet of the mixed flow pump impeller, respectively.

Genetic Aggregation RSM facilitates the optimization of complex, multi-variable problems by systematically selecting the best-performing configurations based on the previous iterations. The optimized blade angle is chosen for additional CFD simulations to validate improvements in performance curves, velocity profiles, and turbulence reduction. Algorithm convergence is carefully evaluated to ensure that refinements lead to stable and meaningful enhancements before finalizing the optimal design.

3. Results and Discussion

3.1 Performance curves and internal flow of mixed flow pump with an initial impeller design

Fig. 10 presents the performance curves of the mixed flow pump with its initial impeller design. The maximum efficiency of 75% is observed at the design flow rate, indicating that the best efficiency point (BEP) aligns with the design point. Fig. 10 shows head drop from 70 m to 20 m over the flow range $0.3 \leq Q/Q_D \leq 1.6$ for the mixed flow pump with semi-open casing. Comparatively, the performance of the mixed flow pump with a semi-open casing is lower than that of an enclosed mixed flow pump. The detailed analysis of hydraulic stability has already been discussed in a previous study[21].

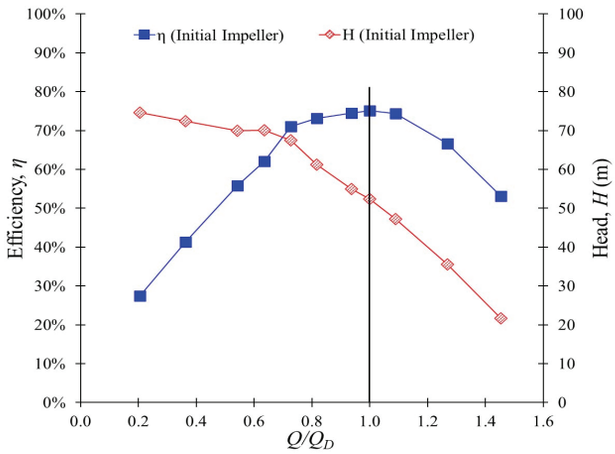

Fig. 10 Performance curves of the mixed flow pump with an initial impeller

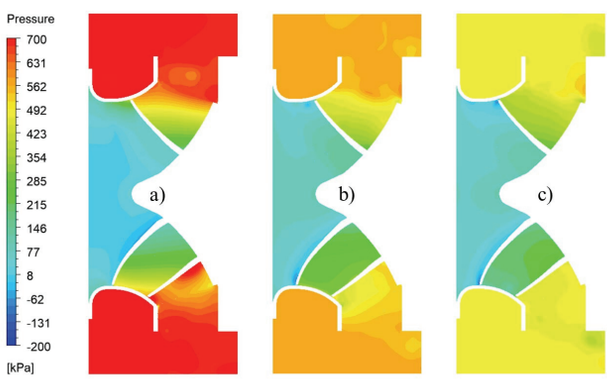

Fig. 11 Comparison of pressure contours in mixed flow pump with initial impeller at a) $Q/Q_D = 0.8$, b) $Q/Q_D = 1.0$ and c) $Q/Q_D = 1.2$

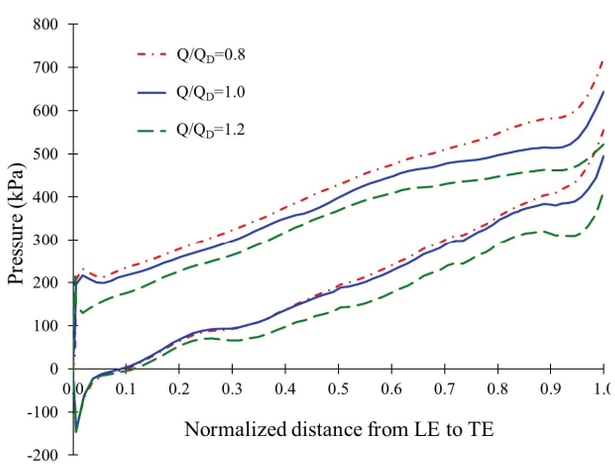

Fig. 12 Pressure distribution in a mixed flow pump with an initial impeller from LE to TE

Fig. 11 shows the pressure contours in the mixed

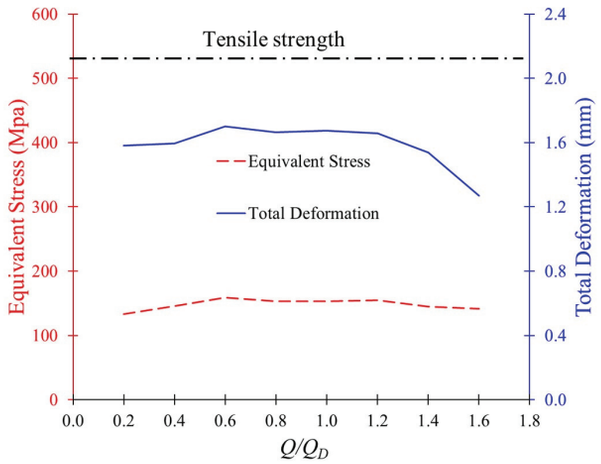

Fig. 13 Equivalent stress and deformation in a mixed flow pump with an initial impeller

flow pump impeller flow passage at various flow conditions. Fig. 12 displays the pressure distribution from LE to TE in the mixed flow pump impeller. The pressure magnitude is gradually increasing from LE to TE. It illustrates that the pressure magnitude is decreasing with an increase in flow rate. Additionally, the FSI analysis is conducted, and Fig. 13 indicates that the equivalent stress is significantly lower than the tensile strength of the stainless steel used for the manufacturing of a mixed flow pump impeller.

3.2 Optimization of mixed flow pump impeller shape

Fig. 14 illustrates the optimal Pareto front between the efficiency and pressure ratio. The Pareto front

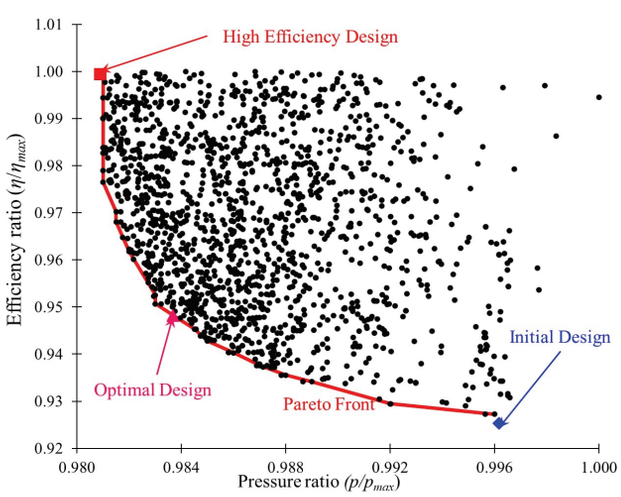

Fig. 14 Selection points along Pareto front for the pump performance optimization by the efficiency trade-off

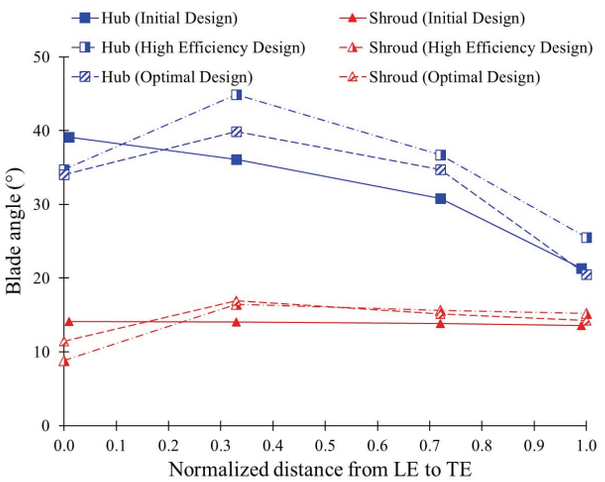

Fig. 15 Blade angle distribution comparison among the initial, high efficiency and optimal impeller designs

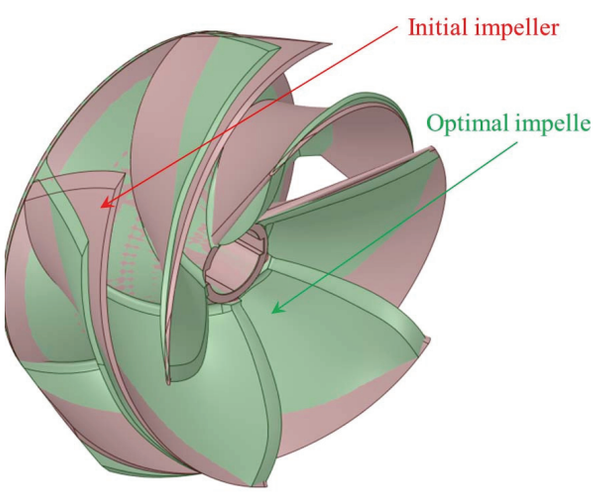

Fig. 16 Comparison of initial and optimal impeller blade shape

represents high efficiency and optimal designs, where the high efficiency design corresponds to the maximum achievable efficiency. The efficiency trade-off plays a crucial role in selecting the optimal impeller design for a mixed flow pump. Fig. 15 compares three impeller designs obtained from the optimal Pareto front. The hub blade angle distribution varies significantly among these designs. Fig. 16 represents the 3D models of the initial and optimal impeller designs.

3.3 Comparison of internal flow characteristics among the impeller designs

The internal flow characteristics of the mixed flow pump are evaluated to compare various impeller

designs. Fig. 17 illustrates the turbulence kinetic energy (*TKE*) distribution within the impeller flow passage under various Q/Q_D. *TKE* is associated with eddies in turbulent flow. At $Q/Q_D = 1.0$, the *TKE* value remains below 4 m^2/s^2 from LE to TE, indicating a low magnitude of eddies at this flow ratio. As the Q/Q_D decreases from 1.0 to 0.4, the *TKE* magnitude increases drastically, signifying the presence of turbulent eddies. The amount of eddies increased significantly when Q/Q_D decreases from 1.0 to 0.4.

Fig. 18 compares TKE and pressure of the initial, high efficiency, and optimal impeller designs at $Q/Q_D = 0.4$. The initial impeller exhibits a higher outlet pressure compared to the high efficiency and optimal impeller designs. The outlet pressure magnitudes are

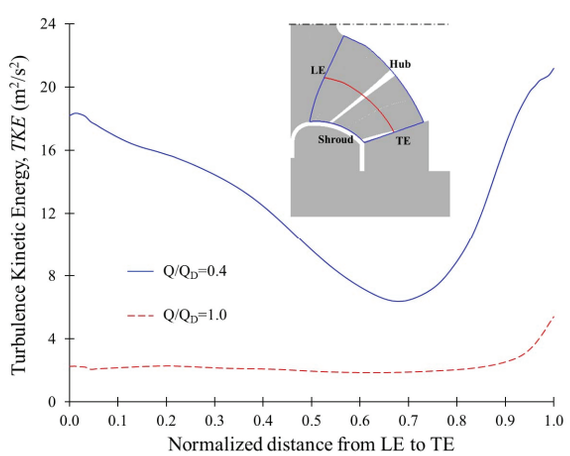

Fig. 17 Comparison of *TKE* at $Q/Q_D = 0.4$ and 1.0 in the initial impeller

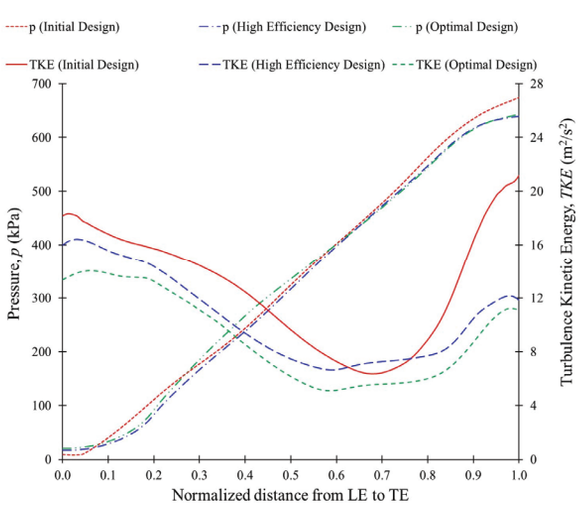

Fig. 18 Comparison of pressure and *TKE* among initial, high efficiency and optimal impeller designs at $Q/Q_D = 0.4$

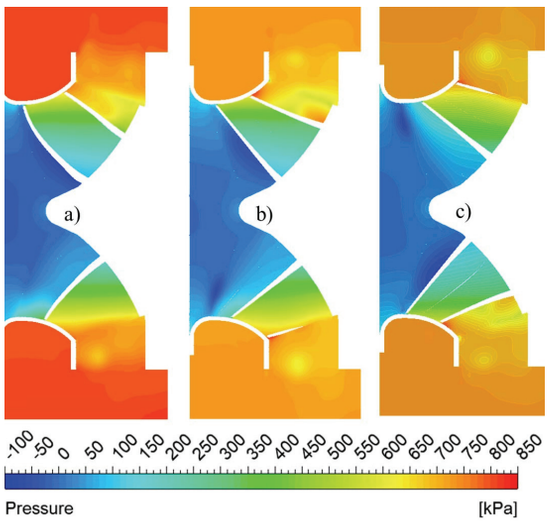

Fig. 19 Comparison of pressure contours in a) initial, b) high efficiency and c) optimal impeller designs at $Q/Q_D = 0.4$

670 kPa, 642 kPa, and 640 kPa for the initial, optimal, and high efficiency impeller designs, respectively. The turbulence kinetic energy (*TKE*) values for the initial, high efficiency, and optimal impeller designs are 18 m^2/s^2, 16 m^2/s^2, and 13 m^2/s^2, respectively, at the LE of the impeller blade. At the TE of the impeller blade, the *TKE* values are 21 m^2/s^2, 12 m^2/s^2, and 11 m^2/s^2 for the initial, high efficiency, and optimal impeller designs, respectively. Fig. 19 illustrates the pressure contours in the cross-section of the mixed flow pump. The initial impeller design maintains a higher outlet pressure compared to the high efficiency and optimal impeller designs.

3.4 Comparison of performance curves between optimal impeller designs

The mixed flow pump with a semi-open casing is designed for specialized applications that operate across a broad range of rotational speeds, particularly during start-up. CFD analysis is conducted to evaluate its performance under varying conditions, over a rotational speed range of 300 min^{-1} to 1200 min^{-1}. Fig. 20 presents the performance curves of the pump with the initial impeller across various flow rates and rotational speeds. The pump's behavior at lower rotational speeds closely reflects its operational characteristics during start-up. The maximum hydraulic efficiency attained with the initial impeller

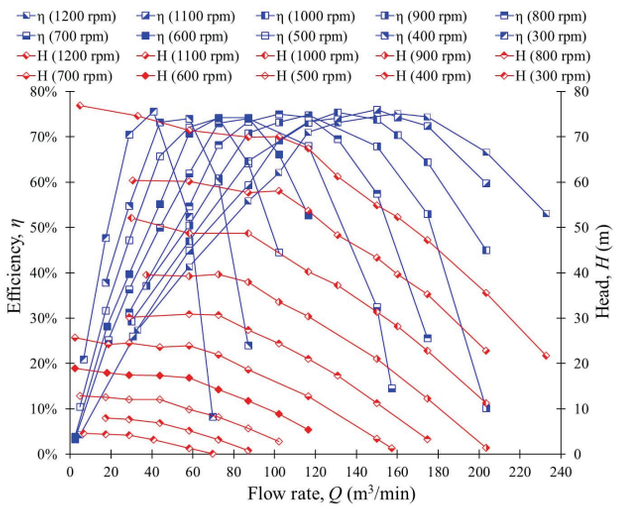

Fig. 20 Performance curves of the initial impeller with various rotational speeds and flow rates

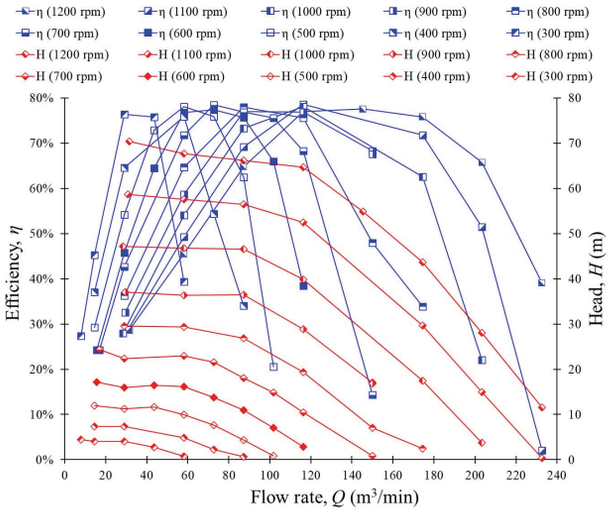

Fig. 22 Performance curves of the optimal impeller with various rotational speeds and flow rates

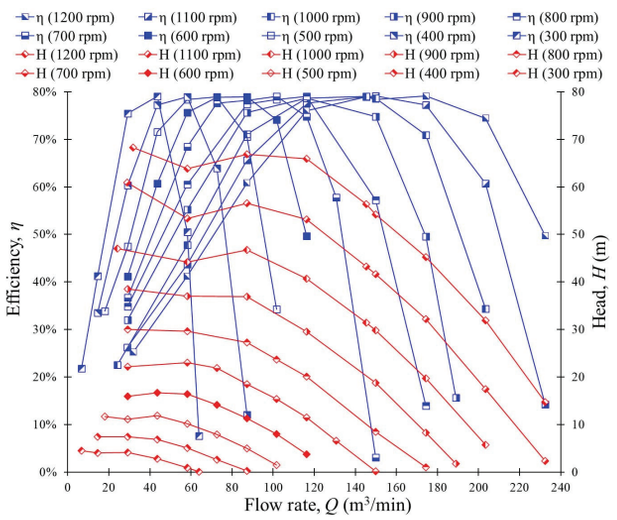

Fig. 21 Performance curves of the high efficiency impeller with various rotational speeds and flow rates

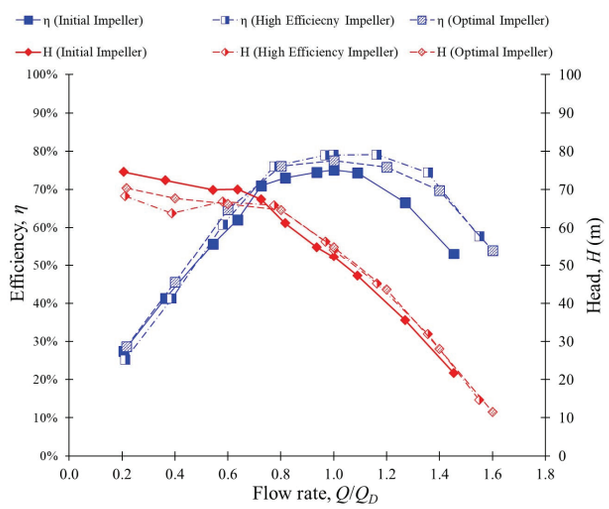

Fig. 23 Performance curves comparison with initial, high efficiency and optimal impellers

is 75%, with efficiency consistently exceeding 72% across all tested speeds, indicating stable and reliable performance throughout the operating range.

As the rotational speed increases, the operating range of the mixed flow pump with a semi-open casing expands. However, at low rotational speeds, the pump operates within a limited flow rate range. The effective head of the mixed flow pump reaches 70 m when operating at 1200 min^{-1} with $Q > 100$ m^3/min. Fig. 21 presents the performance curves of the high efficiency impeller at various rotational speeds. The curves indicate that the best efficiency of 79% is achieved at each rotational speed, demonstrating superior efficiency compared to the initial impeller at the design point. When $N > 1000$ min^{-1} and 30 $m^3/min < Q < 80$ m^3/min, hump characteristics are observed in the mixed flow pump with the high efficiency impeller design, indicating flow instability.

Due to hump characteristics, the mixed flow pump experiences performance fluctuations, efficiency losses, and increased vibration. As a result, selecting a high efficiency impeller design is unsuitable for a wide operational range. Based on the optimal Pareto front and efficiency trade-offs, the optimal impeller design is chosen to mitigate these issues. Fig. 22 presents the performance curves of the mixed flow pump with the

optimal impeller design. The best efficiency achieved with the optimal impeller is 78%, demonstrating a significant suppression of the hump characteristics compared to the high efficiency impeller design. Consequently, the optimal impeller design substantially improves hump characteristics and efficiency compared to both the high efficiency and initial impeller designs.

Fig. 23 compares the initial, high efficiency, and optimal impeller designs. At $Q/Q_D = 1.0$, the efficiencies of the mixed flow pump with the initial, high efficiency, and optimal impeller designs are 75%, 78%, and 79%, respectively. As the flow rate increases from $Q/Q_D = 0.4$ to 0.6, the head values change from 72.40 m to 69.90 m, 63.82 m to 66.82 m, and 67.66 m to 66.18 m for the initial, high efficiency, and optimal impeller designs, respectively. It concludes that the mixed flow pump with the optimal impeller design has better pump efficiency and hump characteristics, making it a suitable choice for enhanced hydraulic stability and operational reliability.

4. Conclusion

The optimization of mixed flow pump impeller design using Computational Fluid Dynamics (CFD), Response Surface Modeling (RSM), and Multi-Objective Genetic Algorithm (MOGA) has demonstrated significant improvements in efficiency and head curve stability. A comparative analysis of the initial, high efficiency, and optimal impeller designs reveals crucial differences in performance. The initial impeller achieved a maximum efficiency of 75% at the design flow rate. The high efficiency impeller improved pump efficiency to 79%, but operational limitations arose due to persistent hump characteristics and performance fluctuations at high rotational speeds. In contrast, the optimal impeller design, refined through the Pareto front analysis and efficiency trade-off, reached 78% efficiency while effectively suppressing hump characteristics, ensuring smoother fluid movement and stable head performance across a wide range of operating conditions. Turbulence kinetic energy analysis showed reduced eddy formation in the optimal impeller, further confirming enhanced hydraulic stability. Additionally, pressure distribution indicated that the initial impeller exhibited high outlet pressure, while the optimal design maintained a balanced pressure profile, minimizing performance fluctuations. The optimal impeller design is developed by integrating CFD, RSM, and MOGA, which enhances performance, suppresses instability, and improves the head curve.

Acknowledgement

이 논문은 2023년 정부(방위사업청)의 재원으로 국방기술진흥연구소의 지원을 받아 수행된 연구임(협약번호 : KRIT-CT-23-002, 고압 압축공기를 이용한 터보펌프 설계 기술)

References

(1) Dash, N., Roy, A. K. and Kumar, K. 2018, “Design and optimization of mixed flow pump impeller blades with hydrostatic loading and varying semi-cone angle,” Materials Today: Proceedings, Vol. 5, No. 5, pp. 11608~11615.

(2) Ji, L., Li, W., Shi, W., Chang, H. and Yang, Z., 2020, “Energy characteristics of mixed-flow pump under different tip clearances based on entropy production analysis,” Energy, Vol. 199, Article No. 117447.

(3) Wang, M., Chen, S., Gu, Y., Yang, Y. Xia, Z., and Chen, J., 2024, “Effect of free and compound vortex designs on the energy characteristics and operational stability of mixed flow pumps,” Physics of Fluids, Vol. 36, No. 8. Article No. 085186

(4) Su, C., Zhang, Z., Zhu, D. and Tao, R. (2025), “Enhancing the Operating Efficiency of Mixed-Flow Pumps Through Adjustable Guide Vanes,” Water, Vol. 17, No. 3, Article No. 423.

(5) Wang, M., Li, Y., Yuan, J. and Yuan, S., 2022, “Effects of different vortex designs on optimization results of mixed-flow pump,” Engineering Applications of Computational Fluid Mechanics, Vol. 16, No. 1, pp. 36~57.

(6) FangFang, H., Peng, W., DaZhuan, W. and LeQin, W., 2014, “Numerical study on the stall behavior of a water jet mixed-flow pump,” Journal of Marine Science and Technology, Vol. 19, pp. 438~449.

(7) Li, W., Li, E., Ji, L., Zhou, L., Shi, W. and Zhu, Y., 2020, “Mechanism and propagation characteristics of rotating stall in a mixed-flow pump,” Renewable Energy, Vol. 153, pp. 74~92.

(8) Zheng, Y., Li, Y., Zhang, F., Yuan, S. and Zhu, X., 2024, “Energy performance improvement for a mixed flow pump based on advanced inlet guide vanes,” Physics of Fluids, Vol. 36, No. 9. Article No. 095143.

(9) Zhang, J., Wang, X., Yang, C., Sun, M. and Huang, Z., 2024, “Investigation on the flow and induced-noise mechanism during the transient start-up process of a

mixed-flow pump," Engineering Computations, Vol. 41, No. 3, pp. 727～754.
(10) Briceño-León, C. X., Iglesias-Rey, P. L., Martinez-Solano, F. J., Mora-Melia, D. and Fuertes-Miquel, V. S., 2021, "Use of fixed and variable speed pumps in water distribution networks with different control strategies," Water, Vol. 13, No. 4, Article No. 479.
(11) Nataraj, M. and Singh, R. R., 2014, "Analyzing pump impeller for performance evaluation using RSM and CFD," Desalination and Water Treatment, Vol. 52, pp. 6822～6831.
(12) Huang, R., Luo, X., Ji, B., Wang, P., Yu, A., Zhai, Z. and Zhou, J., 2015, "Multi-objective optimization of a mixed-flow pump impeller using modified NSGA-II algorithm," Science China technological sciences, Vol. 58, pp. 2122～2130.
(13) Chen, J., Wang, M., Bao, Y., Chen, X. and Xia, H., 2023, "Mixed-flow pump performance improvement based on circulation method," Frontiers in Energy Research, Vol. 11, Article No. 1177437.
(14) Bonaiuti, D. and Zangeneh, M., 2009, "On the coupling of inverse design and optimization techniques for the multiobjective, multipoint design of turbomachinery blades," ASME Journal of Turbomachinery, Vol. 131, No. 2, 021014.
(15) Shrestha, U. and Choi, Y-D., 2020, "A CFD-based shape design optimization process of fixed flow passages in a Francis hydro turbine," Processes, Vol. 8, No. 11, Article No. 1392.
(16) ANSYS Inc., 2024, "ANSYS CFX documentation version 2024R1", http://www.ansys.com.
(17) Menter, F. R., 1994, "Two-equation eddy-viscosity turbulence models for engineering applications," AIAA journal, Vol. 32, No. 8, pp. 1598～1605.
(18) Shrestha, U., Kim, D. and Choi, Y. D., 2024, "Effect of Shaft Sleeve Design on the Hydraulic and Suction Performances of Two-stage Centrifugal Pump," The KSFM Journal of Fluid Machinery, Vol. 27, No. 4, pp. 16～27.
(19) Om Ariara Guhan, C. P., Arthanareeswaran, G., Varadarajan, K. N., & Krishnan, S., 2016, "Numerical optimization of flow uniformity inside an under body-oval substrate to improve emissions of IC engines," Journal of Computational Design and Engineering, Vol. 3, No. 3, pp. 198～214.
(20) Shrestha, U., & Choi, Y. D., 2020, "Improvement of flow behavior in the spiral casing of Francis hydro turbine model by shape optimization," Journal of Mechanical Science and Technology, Vol. 34, No. 9, pp. 3647～3656.
(21) Shrestha, U. and Choi, Y. D., 2024, "Influence of Tip Clearance Gap Thickness on the Performance and Internal Flow of Mixed Flow Pump with Semi-open Casing," The KSFM Journal of Fluid Machinery, Vol. 27, No. 3, pp. 5～13.